Magnetic resonance microimaging of the spinal cord in the SOD1 mouse model of amyotrophic lateral sclerosis detects motor nerve root degeneration

Gary J. Cowin[a]*, Tim J. Butler[b]*, Nyoman D. Kurniawan[a], Charles Watson[c], Robyn H. Wallace[b,d]

[a]Centre for Advanced Imaging, The University of Queensland, Brisbane, Australia

[b]The Queensland Brain Institute , The University of Queensland, Brisbane, Australia

[c]Faculty of Health Sciences, Curtin University, Perth, Australia

[d]The School of Chemistry and Molecular Biosciences, The University of Queensland, Brisbane, Australia

*These authors contributed equally to this work.

Corresponding author: Robyn Wallace, Queensland Brain Institute, The University of Queensland, Brisbane, QLD, 4072, Australia. Email: r.wallace2@uq.edu.au, telephone: +617 3346 6393, fax: +617 3346 6301

Abstract

Amyotrophic lateral sclerosis (ALS) is characterized by selective degeneration of motor neurons. Current imaging studies have concentrated on areas of the brain and spinal cord that contain mixed populations of sensory and motor neurons. In this study, magnetic resonance microimaging (MRM) was used to separate motor and sensory components by visualizing individual dorsal and ventral roots in fixed spinal cords. The high resolution of MRM enabled the axons of pure populations of sensory and motor neurons to be measured in the lumbar region of the SOD1 mouse model of ALS. MRM signal intensity was increased exclusively in the ventral motor nerve roots of the lumbar spinal cord of ALS-affected SOD1 mice compared to wildtype littermates. The hyperintensity was therefore limited to white matter tracts arising from the motor neurons, whereas sensory white matter fibers were unchanged. Significant decreases in ventral nerve root volume were also detected in the SOD1 mice, which correlated with the axonal degeneration observed by microscopy. These results demonstrate the usefulness of MRM in visualising the ultrastructure of the mouse spinal cord. The detailed 3D anatomy allowed the processes of pure populations of sensory and motor neurons to be compared.

Keywords: amyotrophic lateral sclerosis, SOD1, spinal cord magnetic resonance microimaging

1. Introduction

Amyotrophic lateral sclerosis (ALS) is a neurodegenerative disease, in which affected individuals become progressively paralyzed and die within 3 to 5 years (Armon, 1994). ALS is characterized by selective degeneration of large projection neurons or motor neurons in the motor cortex, brainstem and spinal cord. Within the white matter of the spinal cord of ALS patients there is a loss of large myelinated fibers in the corticospinal tracts (Sobue et al., 1987) and ventral roots (Hanyu et al., 1982). The superoxide dismutase 1 (SOD1) transgenic mouse (Gurney et al., 1994) exhibits similar motor neuron degeneration to that observed in human subjects and has become a widely used model for ALS research.

Clinical examination remains the cornerstone of diagnosis for ALS, despite advances in neurophysiology and neuroimaging techniques (Ravits and La Spada, 2009). The inability of these techniques to definitively diagnose ALS may result from the areas of interest containing mixed populations of sensory and motor neurons, diluting the changes occurring primarily in the motor neurons. Pure (or almost pure) populations of sensory or motor neurons occur in the olfactory and optic (sensory) nerves, oculomotor, trochlear, abducens, and hypoglossal (motor) nerves, and the dorsal and ventral roots (sensory and motor respectively) of the spinal cord. During 2010, there have been two single patient case reports describing gadolinium lumbar nerve root enhancement (Luigetti et al., 2010; Young et al., 2010) and one previous case report of cervical nerve roots and brachial plexus enhancement (Rajabally and Jacob, 2008) in probable case of ALS.

Magnetic resonance microscopy (MRM) is an imaging method that has developed into an indispensable technique in translational and preclinical studies of human neurological diseases. In the past, histology has been the primary tool for the

investigation of structures of the central nervous system in normal and altered conditions. However, MRM has unique characteristics that complement histology. MRM is non-destructive and can acquire 3D images of tissue samples or whole organisms, providing gross and fine volumetrics that do not suffer from shrinkage and section distortions, affording the ability to determine the structural relationship between organs and regions within individual organs. The move to higher field magnets to improve signal-to-noise is partially offset by longer T1 times and shorter T2 and T2* relaxation times. Paramagnetic contrast agents are of benefit as they shorten T1, enabling greater signal-to-noise per unit time. These agents can also improve tissue contrast by selection of the contrast agent and use of targeted contrast agents (Bendszus et al., 2008; Blackwell et al., 2009; Huang et al., 2009; Ullmann et al., 2010b). For example, uptake studies by Huang et. al, suggest passive equilibration of Gd-DTPA contrast agent between the bathing solution and tissue. However, Mn^{2+} concentrated in the tissue, suggesting binding of Mg^{2+} to the tissue. Improved tissue contrast and the ability to acquire a single 3D data set also lend themselves to both manual and automatic segmentation. Automated segmentation has been exploited for the generation of anatomic atlases such as the mouse brain (Ali et al., 2005; Johnson et al., 2007; Ma et al., 2005; Ma et al., 2008; Scheenstra et al., 2009; Sharief et al., 2008), rat brain (Schwarz et al., 2006), rhesus monkey (Wisco et al., 2008) and zebrafish (Ullmann et al., 2010a).

Magnetic resonance techniques have been extensively used to assess white matter changes, such as demyelination and axonal injury, in the mouse spinal cord (Pirko and Johnson, 2008). In the experimental allergic encephalomyelitis model of multiple sclerosis, contrast changes have been observed in conventional anatomic images (Schellenberg et al., 2007), axial diffusivity has been correlated with axonal damage (Budde et al., 2008; Budde et al., 2007; Budde et al., 2009), and decreased quantitative T2 and magnetic transfer values have been shown (McCreary et al., 2009). Numerous studies have also assessed white matter integrity in mouse models of spinal cord injury, using diffusion tensor imaging (Kim et al., 2007; Kim et al., 2010; Loy et al., 2007; Tu et al., 2010), T1- and T2-weighted imaging (Gonzalez-Lara et al., 2009; Levene et al.,

2008; Nishi et al., 2007), and MRM (Bilgen, 2007). In mouse models of ALS, MRM has been used to show a decrease in total white matter volume of the spinal cord (Petrik et al., 2007) and our previous studies using *in vivo* diffusion tensor imaging have demonstrated decreased anisotropy that was restricted to ventral regions of the spinal cord (Underwood, unpublished). However, in none of these previous studies of the mouse spinal cord have pure populations of motor neurons been investigated.

We have used MRM to image fixed mouse spinal columns. The resolution obtained in vertebral columns allowed localization of individual dorsal and ventral roots, enabling pure populations of sensory and motor neurons to be compared in normal and a SOD1 transgenic mouse model of ALS. Higher resolution MRM images of short segments of spinal cord were compared with histology and indicated visualisation of white matter tracts and motor neuron pools.

2. Materials and Methods

2.1 Animals and sample preparation

C57BL6 mice overexpressing the human SOD1 transgene carrying the G93A mutation (SOD1 mice) were obtained from The Jackson Laboratory (stock number: 004435). These mice develop symptoms of ALS at approximately 90 days of age and reach end-stage at 145 to 165 days. Control mice were wildtype (WT) C57BL6 littermates of the SOD1 mice, which lacked the SOD1 transgene. SOD1 (n = 7) and WT mice (n = 7) were administered an overdose of sodium pentobarbital (Virbac, Milperra, Australia) at disease end-stage (158 days old) then perfused with 4% paraformaldehyde in phosphate buffered saline (PBS), after which the spinal columns were removed and trimmed down to vertebrae T7 to L4. The same tissue was used for MRI imaging and histological evaluation. A single control mouse, not included in the above control group, was prepared as above and then a ~2.2 mm length of spinal cord at the lumbar enlargement was dissected for ultra-high resolution MRM. The University of Queensland Animal Ethics Committee approved all experiments.

2.2 Magnetic resonance microscopy

The intact spinal columns were washed over three nights in PBS (changed daily) to remove excess fixative before being soaked for a minimum of 24 hours in 0.2% (by volume) Magnevist (Schering AG, Germany), which contains gadopentetate dimeglumine (Gd-DTPA, 4.69g/10ml). Samples were imaged on a Bruker (Karlsruhe, Germany) AV700 magnetic resonance microimaging system consisting of a 16.4T magnet interfaced to an AVANCE II spectrometer running Paravision 4.0 software and MRI data acquired using a 10 mm quadrature radio frequency (RF) coil. The imaging protocol was a 3D gradient echo sequence with the following parameters: TR = 40 ms, TE = 6.5 ms, pulse angle = Ernst angle, number of averages = 5, total imaging time = 15 hr 50 min, field-of-view = 6 X 28 X 6 mm, acquisition matrix = 400 X 854 X 334, zero filled to give an image matrix of 512 X 1024 X 400 for a final image resolution of 12 X 15 μm axial resolution and 27 μm along the cranial/caudal direction.

A short length of extracted mouse spinal cord was prepared as above and imaged on the Bruker AV700. The sample was placed in a 5 mm NMR tube and immersed in fomblin oil. A 5 mm solenoid RF coil was used with the following parameters: TR = 40 ms, TE = 7.3 ms, pulse angle = Ernst angle, number of averages = 22, imaging time = 11 hrs 12 min, field-of-view = 2.56 X 2.56 X 2.56 mm, phase acceleration was used with an acquisition matrix of 256 X 214 X 214 which was zero filled before Fourier transformation to give an image matrix of 256 X 256 X 256 and image resolution of 10 X 10 X 10 μm.

2.3 Image analysis

MR data sets from the spinal column of SOD1 and WT mice were examined using OsiriX v3.6 advanced 3D visualization and volume modelling software (Rosset 2004) to display spinal cord structures. The high spatial resolution of the 3D spinal cord microimages (Fig. 1) allowed determination of anatomical landmarks and points of reference based on the mouse spinal cord atlas (Watson et al., 2009). For calculation of signal intensity (Fig. 2), images from sections transverse to the axis of the spinal cord were analyzed using OsiriX, which was used to partition each data set into different

regions of interest (ROIs). L2 and L3 nerve roots were identified by first locating the L2 and L3 vertebrae, then following the nerve roots to the point where they lay next to the grey matter within the spinal cord (Fig. 2A & 2B). The L2 and L3, ventral and dorsal, nerve root segments were examined separately. For calculation of signal intensities, 5 slices were averaged per spinal column from the L2 and L3 nerve roots. The volumes of the L2 ventral and dorsal nerve roots were measured from the point at which the motor and sensory nerves can be seen as separate entities, just prior to the formation of the L2 spinal nerve. ROI's were then drawn on 20 consecutive slices anterior to the L2 spinal nerve, which were included in the overall volume computation. After image volumes were segmented, corresponding polygonal surface models were generated to provide a 3D representation of the L2 nerve roots (Fig. 5A) using Amira 5.3 advanced 3D visualization and volume modelling software (Visage Imaging Inc., San Diego, CA).

2.4 Histology

Following MRI, spinal columns were decalcified in 15% EDTA for 5 days, dissected down to vertebrae L1 – L2 (the location where the L2 nerve roots are clearly visible as determined by MRM), then embedded in paraffin. Blocks were sectioned at 6 μm and stained with Luxol Fast Blue/Cresyl Violet. Sections were imaged on a Zeiss Axio Imager Z1. The total number of axons was counted in each nerve root using AxioVision software v4.7.1.0 (Carl Zeiss, Germany).

2.5 Statistics

Statistical evaluations of signal intensity and volume measurements were conducted on images from the SOD1 and WT mice. Raw data from MRM signal intensity, nerve root volume, and axon counts for each mouse were pooled to give a mean and SEM for each group. The ventral (motor) nerve root signal intensities were normalised to the dorsal (sensory) nerve roots, to account for variation in intensity between different scans. The means from SOD1 and WT mice were assessed for significance using a paired, two-tailed t-test. Correlations between axon counts and MRM signal intensities were performed using Pearson's Correlation.

3. Results

MRM of the intact mouse spinal column enabled the generation of 3D images with a resolution of 12 X 15 X 27 μm. Detailed anatomy of the spinal cord, nerve roots, vertebra, and surrounding tissue can be clearly visualized (Fig. 1). Imaging the spinal cord within the column facilitated the accurate identification of individual nerve roots, allowing analyses of the axons of pure pools of sensory and motor neurons.

3.1 Motor nerve root signal intensity is increased in SOD1 mice

The MRI intensity of motor nerve roots in the lumbar spinal cord was examined in SOD1 and WT mice (Fig. 2). In WT mice, there was no significant difference between motor and sensory nerve root intensity (Fig. 2A, Fig. 3A) at either L2 ($p = 0.10$) or L3 ($p = 0.25$). In contrast, there was a significant difference between motor and sensory nerve roots intensity in SOD1 mice at both L2 ($p = 0.009$) and L3 ($p = 0.002$), where motor nerve roots showed approximately 25-30% increase in hyperintensity (Fig. 2B, Fig. 3A). When the intensity of the motor nerve roots was normalised against the intensity of the sensory nerve roots (Fig. 3B), the intensity was significantly higher in SOD1 mice compared to controls at both lumbar nerve root L2 ($p = 0.029$) and L3 ($p = 0.027$). Histological examination of the spinal cords and adjacent nerve roots showed decreased axon density and a general decrease in membrane density in SOD1 mice (Fig. 2E & 2F). The normalised MRM intensity of L2 and L3 nerve roots in SOD1 mice increased by 38.3% and corresponded to a 27.4% loss of axons as determined by histology. There was a strong correlation between axon number and MRM intensity at the L2 ($r^2 = 0.77$, $p = 0.02$) motor nerve root (Fig. 4). Severe shrinkage of tissue following histological staining was evident (Fig. 2C & 2D).

3.2 Motor nerve root volume is decreased in SOD1 mice

The volume of the L2 ventral root was measured from the point at which the motor and sensory roots can be seen as separate entities, just prior to the formation of the ganglion (Fig. 5). SOD1 mice had a significantly decreased ventral root volume

compared to WT ($p = 0.01$), which was only observed in the ventral root and not the L2 dorsal root ($p = 0.79$).

3.3 MRM reveals ultrastructures of the spinal cord

A single short segment of the lumbar mouse spinal cord and adjacent nerve roots was imaged to give an isotropic resolution of 10 μm. Minimum and maximum intensity projections through 8 slices were generated in OsiriX to emphasize the ultrastructure that can be visualized within the mouse spinal cord (Fig. 6). The images were cross-referenced against the appearance of the spinal cord from a histological mouse spinal cord atlas (Fig. 6A; Watson et al., 2009). The minimum intensity image (Fig. 6B) highlights the transverse and longitudinal white matter tracts within the grey matter spinal cord. Intense regions in the grey matter of the maximum intensity image (Fig. 6C) correlate well with the location of motor neuron pools found in AChE stained sections (Fig. 6A). White matter fibers projecting from the grey matter are also clearly visible in the maximum intensity image (Fig. 6C).

4. Discussion

We have shown the utility of MRM of intact mouse spinal column samples to visualise the formation of individual motor and sensory nerve roots, then follow the combination of the motor and sensory axons in the spinal ganglion to form the nerves that extend throughout the body. The imaging was performed without destruction of the bony structures or tissue around the spinal column, and with minimal shrinkage and distortion of tissue. This gives a unique ability to visualize and assess the structural relationship between the different components of the spinal cord, as it exists in the living animal.

The SOD1 transgenic mouse was employed in this study as a model neurodegenerative condition resulting from loss of motor neuron integrity. In-plane image resolution of 15 μm in intact spinal cord segments allowed clear visualization of the individual dorsal and ventral nerve roots. The 10 μm ultrahigh resolution imaging facilitated the

assessment of pure pools of motor and sensory axons, allowing the identification of changes that were localized to the axons of motor neurons and independent of the sensory nerve roots and spinal cord white matter.

Several human MRI studies in ALS patients have been performed, with the most consistent finding being increased signal intensity in the corticospinal tract (Cheung et al., 1995; da Rocha et al., 2004; Ellis et al., 1999; Friedman and Tartaglino, 1993; Goodin et al., 1988; Luis et al., 1990; Marti-Fabregas and Pujol, 1990), and lateral spinal cord (Mascalchi et al., 1995). Three single patient case reports have described gadolinium enhancement of nerve roots (Luigetti et al., 2010; Rajabally and Jacob, 2008; Young et al., 2010). The MRM finding of increased signal intensity in the SOD1 mouse ventral spinal cord white matter reported here is consistent with the three case reports in humans. The increased signal intensity correlated with axon damage and myelin loss as observed by histology (Fig. 2 & 3). Assessment of histological changes has not been reported in human cases with gadolinium nerve root enhancement.

The importance of this report lies in the comparison of pure populations of sensory and motor neurons. The MRM-visible intensity changes observed in the SOD1 mice were limited to the the axons of motor neurons in the ventral roots. It is unclear if the presence of the gadolinium contrast agent increases the intensity changes beyond a general improvement in signal-to-noise. Huang et al. (2009) reported passive uptake of Gd-DTPA but non-uniform tissue distribution. In contrast, Mn^{2+} exhibited evidence for protein and macromolecule binding. Different tissue contrast between Gd-DTPA and Mn^{2+} was illustrated. Gadofluorine contrast agents have shown greater ability to enhance multiple sclerosis hyperintensities than Gd-DTPA (Bendszus et al., 2008). Together, these results illustrate the potential for specialized MR contrast agents, similar to the array of cell specific stains currently used in histology.

This has been the first study to use MRM in the mouse spinal cord to detect nerve root volume loss (Fig. 5). The relative thickness of the white matter in the spinal cord and the nerve roots changes dramatically along the spinal cord. Previous *in vivo* imaging

has not clearly differentiated the spinal cord white matter and the nerve roots (Bilgen et al., 2005). However only slices anterior to vertebra T12 was shown, where the nerve roots are still small compared to the cord white matter. The lack of resolution in previous MRI studies could result in a region of interest containing both cord white matter and nerve root tissue. In cases where the change is evident only in the ventral nerve root, combining the cord white matter and ventral nerve root would reduce the ability to detect a change.

The resolution achieved by MRM increases with smaller coil size and correspondingly smaller samples (Ciobanu et al., 2003). This was illustrated by the MRM images obtained from a small segment of fixed spinal cord in a 5 mm solenoid coil (Fig. 6). Isotropic image resolution of 10 μm allowed close to optical microscopy resolution. The architecture of the white matter, the white matter tracts within the grey matter and motoneuron pools were visible. This resolution was achieved in the intact piece of tissue without the need to section the sample.

5. Conclusions

MRM was effective in comparing the anatomy of individual dorsal and ventral nerve roots, allowing pure populations of sensory and motor neurons to be compared in the intact mouse spinal column. Ventral nerve root degeneration in SOD1 mice was visualised as reduced nerve root volume and increased image intensity, with no changes detected in the dorsal nerve roots. Compared to conventional histology, MRM has the ability to view the spinal column in three dimensions with minimal tissue disruption and shrinkage.

Acknowledgements

Funding provided by the Ross Maclean Fellowship, Peter Goodenough Bequest and the Queensland Nuclear Magnetic Resonance Network. Jane Ellis for assistance with histology.

References

Ali, A.A., Dale, A.M., Badea, A., Johnson, G.A., 2005. Automated segmentation of neuroanatomical structures in multispectral MR microscopy of the mouse brain. Neuroimage 27, 425-435.
Armon, C., 1994. Motor Neuron Disease. Marcel Dekker, New York.
Bendszus, M., Ladewig, G., Jestaedt, L., Misselwitz, B., Solymosi, L., Toyka, K., Stoll, G., 2008. Gadofluorine M enhancement allows more sensitive detection of inflammatory CNS lesions than T2-w imaging: a quantitative MRI study. Brain 131, 2341-2352.
Bilgen, M., 2007. Magnetic resonance microscopy of spinal cord injury in mouse using a miniaturized implantable RF coil. J Neurosci Methods 159, 93-97.
Bilgen, M., Al-Hafez, B., Berman, N.E., Festoff, B.W., 2005. Magnetic resonance imaging of mouse spinal cord. Magn Reson Med 54, 1226-1231.
Blackwell, M.L., Farrar, C.T., Fischl, B., Rosen, B.R., 2009. Target-specific contrast agents for magnetic resonance microscopy. Neuroimage 46, 382-393.
Budde, M.D., Kim, J.H., Liang, H.F., Russell, J.H., Cross, A.H., Song, S.K., 2008. Axonal injury detected by in vivo diffusion tensor imaging correlates with neurological disability in a mouse model of multiple sclerosis. NMR Biomed 21, 589-597.
Budde, M.D., Kim, J.H., Liang, H.F., Schmidt, R.E., Russell, J.H., Cross, A.H., Song, S.K., 2007. Toward accurate diagnosis of white matter pathology using diffusion tensor imaging. Magn Reson Med 57, 688-695.
Budde, M.D., Xie, M., Cross, A.H., Song, S.K., 2009. Axial diffusivity is the primary correlate of axonal injury in the experimental autoimmune encephalomyelitis spinal cord: a quantitative pixelwise analysis. J Neurosci 29, 2805-2813.
Cheung, G., Gawel, M.J., Cooper, P.W., Farb, R.I., Ang, L.C., Gawal, M.J., 1995. Amyotrophic lateral sclerosis: correlation of clinical and MR imaging findings. Radiology 194, 263-270.
Ciobanu, L., Webb, A., G. , Pennington, C., H. , 2003. Magnetic resonance imaging of biological cells. Progress in Nuclear Magnetic Resonance Spectroscopy 42, 69-93.
da Rocha, A.J., Oliveira, A.S., Fonseca, R.B., Maia, A.C., Jr., Buainain, R.P., Lederman, H.M., 2004. Detection of corticospinal tract compromise in amyotrophic lateral sclerosis with brain MR imaging: relevance of the T1-weighted spin-echo magnetization transfer contrast sequence. AJNR Am J Neuroradiol 25, 1509-1515.
Ellis, C.M., Simmons, A., Dawson, J.M., Williams, S.C., Leigh, P.N., 1999. Distinct hyperintense MRI signal changes in the corticospinal tracts of a patient with motor neuron disease. Amyotroph Lateral Scler Other Motor Neuron Disord 1, 41-44.
Friedman, D.P., Tartaglino, L.M., 1993. Amyotrophic lateral sclerosis: hyperintensity of the corticospinal tracts on MR images of the spinal cord. AJR Am J Roentgenol 160, 604-606.
Gonzalez-Lara, L.E., Xu, X., Hofstetrova, K., Pniak, A., Brown, A., Foster, P.J., 2009. In vivo magnetic resonance imaging of spinal cord injury in the mouse. J Neurotrauma 26, 753-762.
Goodin, D.S., Rowley, H.A., Olney, R.K., 1988. Magnetic resonance imaging in amyotrophic lateral sclerosis. Ann Neurol 23, 418-420.

Gurney, M.E., Pu, H., Chiu, A.Y., Dal Canto, M.C., Polchow, C.Y., Alexander, D.D., Caliendo, J., Hentati, A., Kwon, Y.W., Deng, H.X., et al., 1994. Motor neuron degeneration in mice that express a human Cu,Zn superoxide dismutase mutation. Science 264, 1772-1775.
Hanyu, N., Oguchi, K., Yanagisawa, N., Tsukagoshi, H., 1982. Degeneration and regeneration of ventral root motor fibers in amyotrophic lateral sclerosis. Morphometric studies of cervical ventral roots. J Neurol Sci 55, 99-115.
Huang, S., Liu, C., Dai, G., Kim, Y.R., Rosen, B.R., 2009. Manipulation of tissue contrast using contrast agents for enhanced MR microscopy in ex vivo mouse brain. Neuroimage 46, 589-599.
Johnson, G.A., Ali-Sharief, A., Badea, A., Brandenburg, J., Cofer, G., Fubara, B., Gewalt, S., Hedlund, L.W., Upchurch, L., 2007. High-throughput morphologic phenotyping of the mouse brain with magnetic resonance histology. Neuroimage 37, 82-89.
Kim, J.H., Loy, D.N., Liang, H.F., Trinkaus, K., Schmidt, R.E., Song, S.K., 2007. Noninvasive diffusion tensor imaging of evolving white matter pathology in a mouse model of acute spinal cord injury. Magn Reson Med 58, 253-260.
Kim, J.H., Loy, D.N., Wang, Q., Budde, M.D., Schmidt, R.E., Trinkaus, K., Song, S.K., 2010. Diffusion tensor imaging at 3 hours after traumatic spinal cord injury predicts long-term locomotor recovery. J Neurotrauma 27, 587-598.
Levene, H.B., Mohamed, F.B., Faro, S.H., Seshadri, A.B., Loftus, C.M., Tuma, R.F., Jallo, J.I., 2008. Small mammal MRI imaging in spinal cord injury: a novel practical technique for using a 1.5 T MRI. J Neurosci Methods 172, 245-249.
Loy, D.N., Kim, J.H., Xie, M., Schmidt, R.E., Trinkaus, K., Song, S.K., 2007. Diffusion tensor imaging predicts hyperacute spinal cord injury severity. J Neurotrauma 24, 979-990.
Luigetti, M., Cianfoni, A., Conte, A., Sabatelli, M., 2010. Gadolinium enhancement of the lumbar leptomeninges and roots in a case of ALS. Amyotroph Lateral Scler 11, 412-413.
Luis, M.L., Hormigo, A., Mauricio, C., Alves, M.M., Serrao, R., 1990. Magnetic resonance imaging in motor neuron disease. J Neurol 237, 471-474.
Ma, Y., Hof, P.R., Grant, S.C., Blackband, S.J., Bennett, R., Slatest, L., McGuigan, M.D., Benveniste, H., 2005. A three-dimensional digital atlas database of the adult C57BL/6J mouse brain by magnetic resonance microscopy. Neuroscience 135, 1203-1215.
Ma, Y., Smith, D., Hof, P.R., Foerster, B., Hamilton, S., Blackband, S.J., Yu, M., Benveniste, H., 2008. In Vivo 3D Digital Atlas Database of the Adult C57BL/6J Mouse Brain by Magnetic Resonance Microscopy. Front Neuroanat 2, 1.
Marti-Fabregas, J., Pujol, J., 1990. Selective involvement of the pyramidal tract on magnetic resonance imaging in primary lateral sclerosis. Neurology 40, 1799-1800.
Mascalchi, M., Salvi, F., Valzania, F., Marcacci, G., Bartolozzi, C., Tassinari, C.A., 1995. Corticospinal tract degeneration in motor neuron disease. AJNR Am J Neuroradiol 16, 878-880.

McCreary, C.R., Bjarnason, T.A., Skihar, V., Mitchell, J.R., Yong, V.W., Dunn, J.F., 2009. Multiexponential T2 and magnetization transfer MRI of demyelination and remyelination in murine spinal cord. Neuroimage 45, 1173-1182.
Nishi, R.A., Liu, H., Chu, Y., Hamamura, M., Su, M.Y., Nalcioglu, O., Anderson, A.J., 2007. Behavioral, histological, and ex vivo magnetic resonance imaging assessment of graded contusion spinal cord injury in mice. J Neurotrauma 24, 674-689.
Petrik, M.S., Wilson, J.M., Grant, S.C., Blackband, S.J., Tabata, R.C., Shan, X., Krieger, C., Shaw, C.A., 2007. Magnetic resonance microscopy and immunohistochemistry of the CNS of the mutant SOD murine model of ALS reveals widespread neural deficits. Neuromolecular Med 9, 216-229.
Pirko, I., Johnson, A.J., 2008. Neuroimaging of demyelination and remyelination models. Curr Top Microbiol Immunol 318, 241-266.
Rajabally, Y.A., Jacob, S., 2008. Chronic inflammatory demyelinating polyneuropathy-like disorder associated with amyotrophic lateral sclerosis. Muscle Nerve 38, 855-860.
Ravits, J.M., La Spada, A.R., 2009. ALS motor phenotype heterogeneity, focality, and spread: deconstructing motor neuron degeneration. Neurology 73, 805-811.
Scheenstra, A.E., van de Ven, R.C., van der Weerd, L., van den Maagdenberg, A.M., Dijkstra, J., Reiber, J.H., 2009. Automated segmentation of in vivo and ex vivo mouse brain magnetic resonance images. Mol Imaging 8, 35-44.
Schellenberg, A.E., Buist, R., Yong, V.W., Del Bigio, M.R., Peeling, J., 2007. Magnetic resonance imaging of blood-spinal cord barrier disruption in mice with experimental autoimmune encephalomyelitis. Magn Reson Med 58, 298-305.
Schwarz, A.J., Danckaert, A., Reese, T., Gozzi, A., Paxinos, G., Watson, C., Merlo-Pich, E.V., Bifone, A., 2006. A stereotaxic MRI template set for the rat brain with tissue class distribution maps and co-registered anatomical atlas: application to pharmacological MRI. Neuroimage 32, 538-550.
Sharief, A.A., Badea, A., Dale, A.M., Johnson, G.A., 2008. Automated segmentation of the actively stained mouse brain using multi-spectral MR microscopy. Neuroimage 39, 136-145.
Sobue, G., Hashizume, Y., Mitsuma, T., Takahashi, A., 1987. Size-dependent myelinated fiber loss in the corticospinal tract in Shy-Drager syndrome and amyotrophic lateral sclerosis. Neurology 37, 529-532.
Tu, T.W., Kim, J.H., Wang, J., Song, S.K., 2010. Full tensor diffusion imaging is not required to assess the white-matter integrity in mouse contusion spinal cord injury. J Neurotrauma 27, 253-262.
Ullmann, J.F., Cowin, G., Kurniawan, N.D., Collin, S.P., 2010a. A three-dimensional digital atlas of the zebrafish brain. Neuroimage 51, 76-82.
Ullmann, J.F., Cowin, G., Kurniawan, N.D., Collin, S.P., 2010b. Magnetic resonance histology of the adult zebrafish brain: optimization of fixation and gadolinium contrast enhancement. NMR Biomed 23, 341-346.
Watson, C., Paxinos, G., Kayalioglu, G., Heise, C., 2009. Atlas of the mouse spinal cord. In: Watson, C., Paxinos, G., Kayalioglu, G. (Eds.), The Spinal Cord. A

Christopher and Dana Reeve Foundation Text and Atlas Elsevier Academic Press, San Diego, pp. 308-379.
Wisco, J.J., Rosene, D.L., Killiany, R.J., Moss, M.B., Warfield, S.K., Egorova, S., Wu, Y., Liptak, Z., Warner, J., Guttmann, C.R., 2008. A rhesus monkey reference label atlas for template driven segmentation. J Med Primatol 37, 250-260.
Young, N.P., Laughlin, R.S., Sorenson, E.J., 2010. Gadolinium enhancement of the lumbar roots in a case of ALS. Amyotroph Lateral Scler 11, 207-209.

Figure Legends

Figure 1. Representative MRM images of the mouse spinal column. This figure shows the overall composition of the mouse spinal column and highlights the anatomical structures used to identify specific nerve roots. A = sagittal; B = coronal; C = horizontal.

Figure 2. *Ex vivo* MRM and histology of WT (A, C, E) and SOD1 (B, D, F) mouse spinal column. A & B) MRM images with L2 dorsal (red) and L2 ventral (green) roots outlined; C & D) Luxol blue/cresyl violet histology at 5x magnification, * = L2 ventral nerve root; E & F) Luxol blue/cresyl violet histology of the L2 ventral nerve root at 40x magnification.

Figure 3. MRM intensity calculations from WT and SOD1 lumbar nerve roots. A) Graph of MRM raw intensity values; B) Motor nerve root intensities normalised to the dorsal nerve roots intensities.

Figure 4. Correlation between MRM intensity and axon number at the L2 ventral nerve root.

Figure 5. Ventral nerve root volumes of wildtype and SOD1 mice. . A) Dorsal (green) and ventral (purple) L2 nerve roots highlighted on MRM image; B) L2 ventral nerve root volume is decreased in SOD1 mice.

Figure 6. MRM of the lumbar mouse spinal cord at a resolution of 10 μm compared to light microscopy. A) Acetylcholinesterase (AChE) staining of a 40 μm histological section (from Watson et al., 2009); B) Maximum intensity MRM image; C) Minimum intensity MRM image. Ps9 = psoas motor neurons; Q9 = quadriceps motor neurons; Ad9 = adductor motor neurons.

1

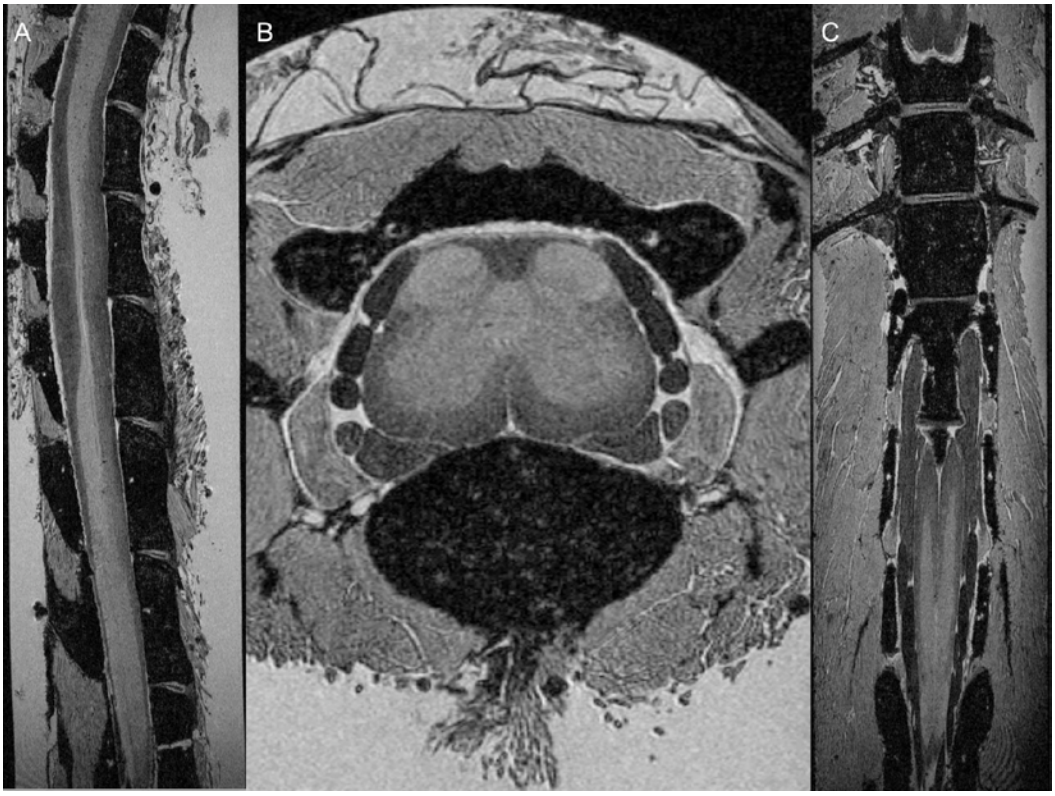

2

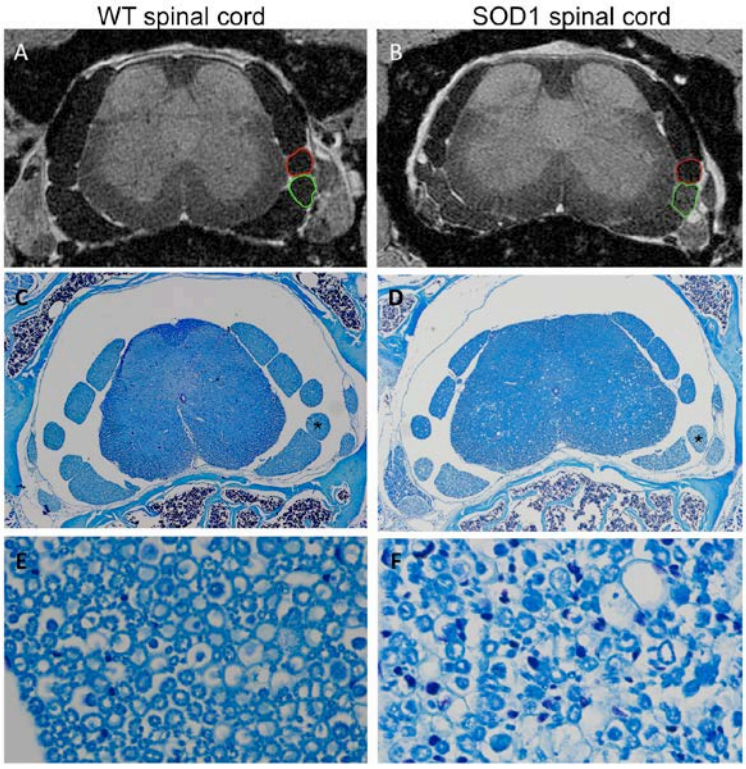

3

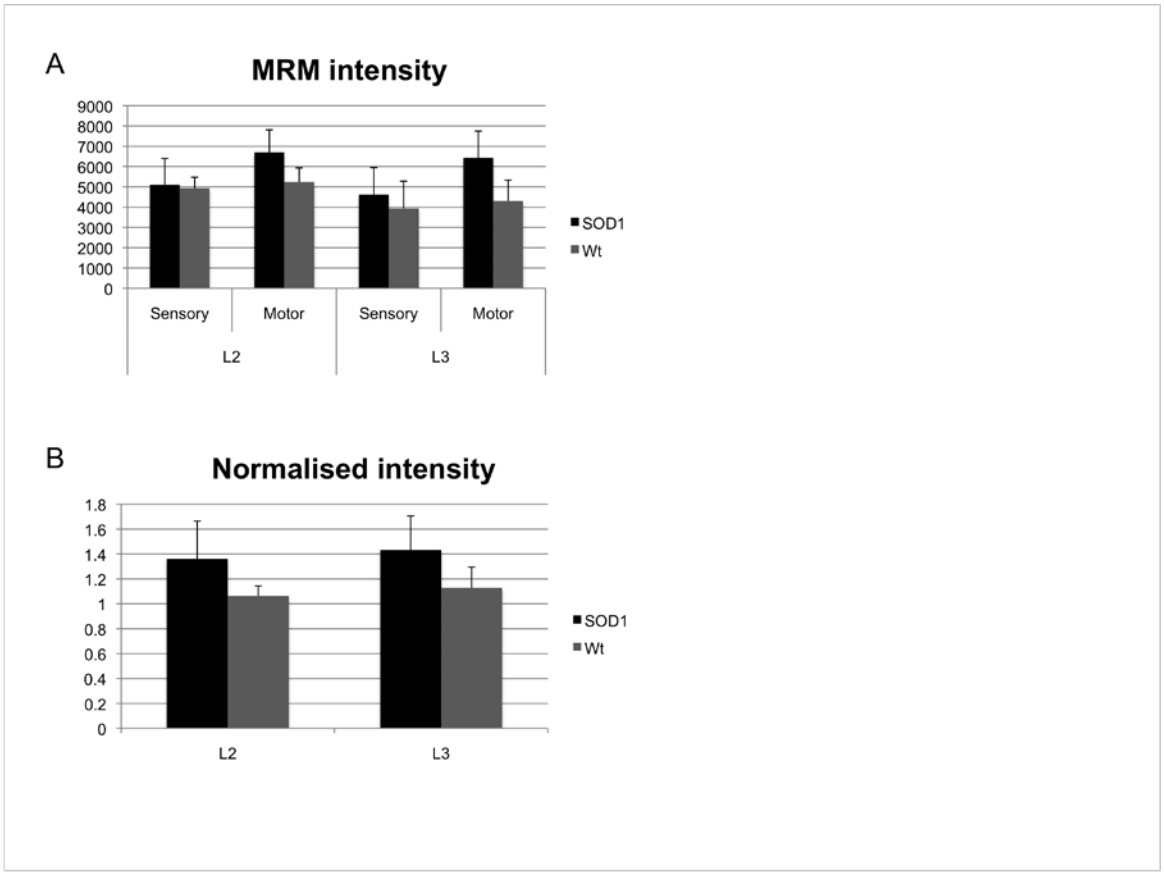
A
MRM intensity
9000
8000
7000
6000
5000
4000
3000
2000
1000
0
Sensory
Motor
Sensory
Motor
L2
L3
SOD1
Wt
B
Normalised intensity
1.8
1.6
1.4
1.2
1
0.8
0.6
0.4
0.2
0
L2
L3
SOD1
Wt

4

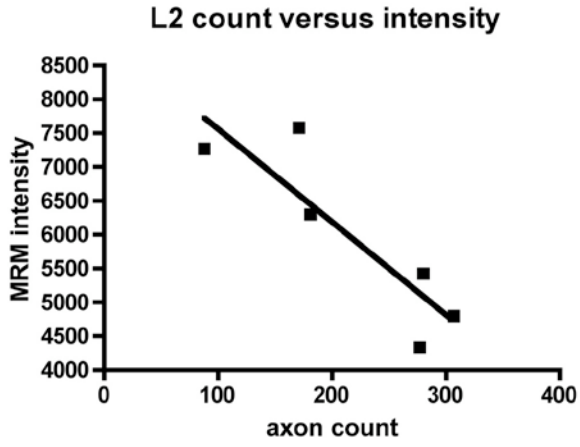
L2 count versus intensity
MRM intensity
8500
8000
7500
7000
6500
6000
5500
5000
4500
4000
0
100
200
300
400
axon count

5

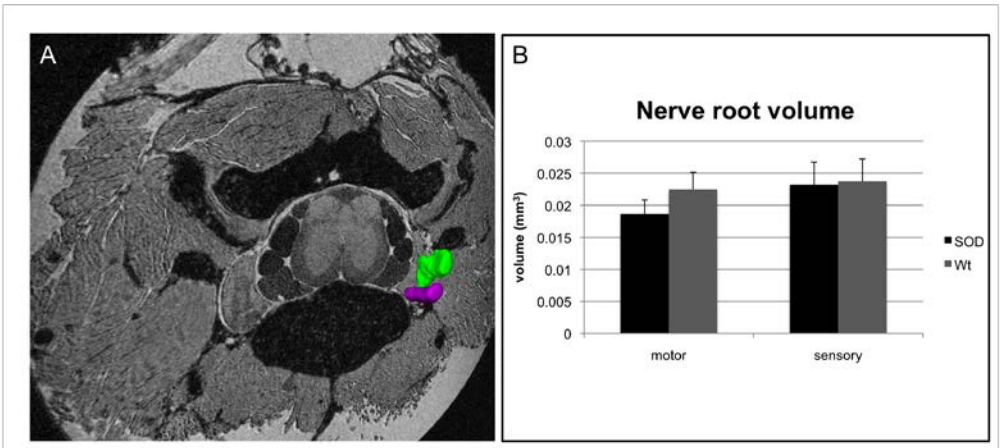
A
B
Nerve root volume
0.03
0.025
0.02
0.015
0.01
0.005
0
volume (mm³)
motor
sensory
SOD
Wt

6

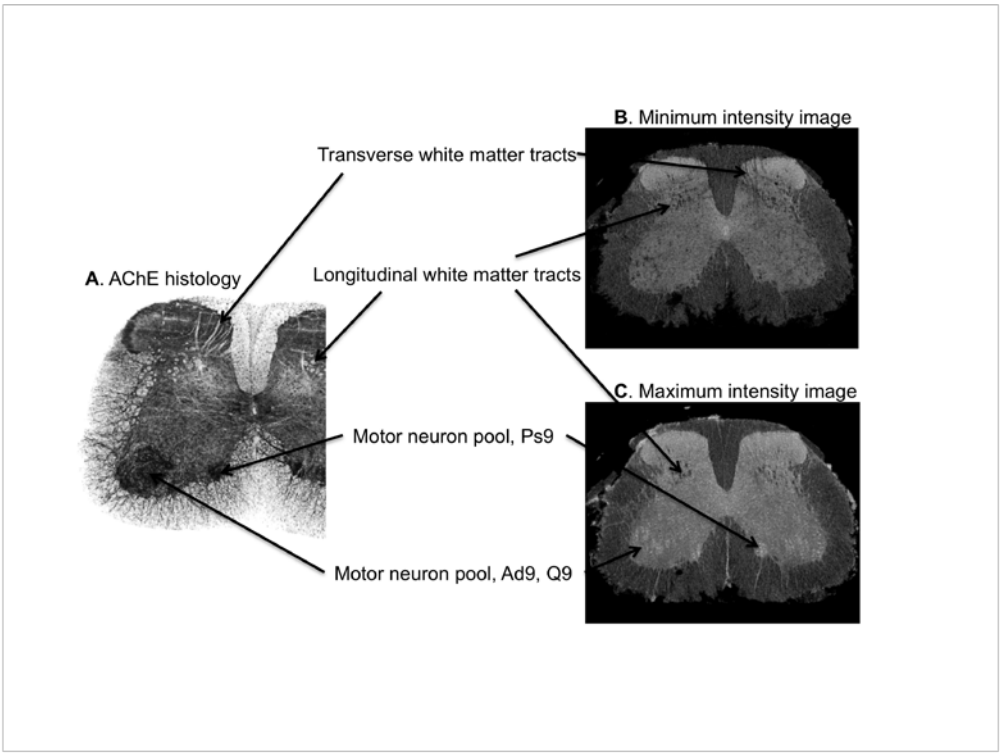
B. Minimum intensity image
Transverse white matter tracts
A. AChE histology
Longitudinal white matter tracts
C. Maximum intensity image
Motor neuron pool, Ps9
Motor neuron pool, Ad9, Q9